# Historic carbon burial spike in an Amazon floodplain lake linked to riparian deforestation near Santarem, Brazil

Luciana M. Sanders[1], Kathryn Taffs[1], Debra Stokes[2], Christian J. Sanders[3], Alex Enrich-Prast[4,5], Leonardo Nogueira Amora[6,7], Humberto Marotta[6,7]

[1]*Southern Cross Geoscience, Southern Cross University, P.O. Box 157, Lismore, NSW 2480, Australia.*
[2]*Marine Ecology Research Centre, Southern Cross University, P.O. Box 157, Lismore, NSW 2480, Australia University, P.O. Box 157, Lismore, NSW 2480, Australia.*
[3]*National Marine Science Centre, School of Environment, Science and Engineering, Southern Cross University, Coffs Harbour, New South Wales, Australia.*
[4]*Laboratório de Biogeoquímica, Universidade Federal do Rio de Janeiro (UFRJ), Rio d Janeiro (RJ), 21941 971, Brazil.*
[5]*Department of Environmental Change, Linköping University, 581 83, Linköping, Sweden.*
[6]*Ecosystems and Global Change Laboratory (LEMG-UFF) / International Laboratory of Global Change (LINCGlobal). Biomass and Water Management Research Center (NAB-UFF). Graduated Program in Geosciences (Environmental Geochemistry). Universidade Federal Fluminense (UFF), Av. Edmundo March, s/nº – Zip Code: 24210-310, Niteroi/RJ- Brazil.*
[7]*Sedimentary and Environmental Processes Laboratory (LAPSA-UFF). Department of Geography. Graduated Program in Geography. Universidade Federal Fluminense (UFF), Av. Gal. Milton Tavares de Souza, s/nº - Zip Code: 24210-346, Niteroi/RJ- Brazil.*

*Corresponding author. E-mail address; l.sanders.13@student.scu.edu.au

**Abstract**

The forests along the Amazon Basin produce significant quantities of organic material, a portion of which is deposited in floodplain lakes. However, potentially important effects of ongoing deforestation in the watershed on these carbon fluxes is still poorly understood. Here, a sediment core was extracted from an Amazon floodplain lake to examine the relationship between carbon burial and land cover/use. Historical records from 1934 and satellite data from 1975 were used to calculate deforestation rates between 1934 and 1975, and 1975 to 2008 in four zones with different distances from the margins of the lake and its tributaries (100, 500, 1000 and 6000-m buffers). Sediment accumulation rates were determined from the $^{240+239}$Pu signatures and the excess $^{210}$Pb method, reaching near 3.8 and 4.2 mm year$^{-1}$ in the last ~60 and ~120 years respectively. The carbon burial rates ranged between 91 and 319 g C m$^{-2}$ year$^{-1}$, with pulses of high carbon burial originates from the forest vegetation, as indicated by $\delta^{13}$C and $\delta^{15}$N signatures in the 1940s and 50s. Our results revealed a potentially important spatial dependence of the OC burial in Amazon lacustrine sediments in relation to deforestation rates in the catchment. These deforestation rates were more intense in the riparian vegetation (100-m buffer) during the period 1934-1975 and the larger open water areas (500, 1000 and 6000-m buffer) during 1975-2008. The continued removal of vegetation from the interior of the forest was not related to the peak of OC burial in the lake, but only the riparian deforestation which peaked during the 1950s. Our novel findings suggest the importance of abrupt and temporary events in which some of the biomass released by the deforestation, especially restricted to areas along open water edges, might reach the depositional environments in the floodplain of the Amazon Basin.

## 1. Introduction

Rivers act as vectors, transporting sediment from land to ocean (Abril et al. 2014). Along this trajectory a significant proportion of the sediment load, including organic material, may be deposited in floodplains, creating zones of carbon accumulation (Smith et al. 2002, Dong et al. 2012, Hoffmann et al. 2013). This process is accelerated during flood events, when rivers and tributaries deposit organic material along the inundated floodplains (Smith et al. 2002). In some climate zones, floodplains are seasonally inundated, with riparian zone vegetation dependent upon this seasonal influx of organic material. The riparian vegetation slows water velocity and traps fine-grained, carbon rich sediments within this low-energy environment (Aalto et al. 2003). Therefore, the riparian vegetation along the floodplains may be important for the organic matter deposition and the Amazon carbon cycle.

The importance of tropical wetland ecosystems in the carbon cycle is well documented (Downing et al. 1993, Melack et al. 2004, Zocatelli et al. 2013, Abril et al. 2014, Marotta et al. 2014). It has been shown that wetlands in the warm tropics are some of the most productive biological communities in the world (Neue et al. 1997), representing an important sink for nutrients (Marotta et al. 2009) and carbon (Peixoto et al. 2016), as well as sources of organic substrates to carbon gas production in inland waters (Marotta et al. 2010). However, these wetland ecosystems are also highly threatened by land use activities, especially from deforestation, development of agricultural land and soil degradation (Junk 2013, Lucas et al. 2014). For example, the Amazon Basin wetlands are being degraded by farming activities such as commercial ranching, and an increase in road density (Goulding 1993).

Deforestation of the Amazon Basin accelerated toward the end of the 1970's (Skole and Tucker 1993), when an estimated 15% of the pristine rainforest area was lost by the year 2003, increasing to approximately 18% by 2015 (INPE 2016). The ongoing loss of vegetation is responsible for a substantial increase in erosion rates and subsequent sediment inputs into Amazon rivers and lakes (Neill et al. 2013b). Yet these anthropogenic activities are potential sources of allochthonous organic matter that may increase carbon stores in the associated floodplain areas (Diaz and Rosenberg 2008, Stanley et al. 2012).

Jupindá Lake provides an ideal opportunity to investigate historical changes in organic carbon burial in a floodplain lake as a result of the well documented anthropogenic activities. This will aid in identifying the still-little known impacts of land cover changes on recent carbon burial rates in depositional environments of the Amazon floodplain. The objectives of this research are to investigate the affects of deforestation and urban development on carbon burial rates in a tropical floodplain lake. We hypothesize that the well documented records on historical deforestation in this region of the Amazon Basin is related to the carbon burial capacity of the floodplain lakes.

## 2. Methods

The city of Santarem, in central Amazon, was established in the mid-eighteenth century, approximately 650 km upstream from the Amazon River mouth and at its confluence with the Tapajós River (02°25'0.28"S and 54°42'41.57"W, Figure 1). In 1940, Santarém was only a small village, less than 0.5 $km^2$, surrounded by dense pristine rainforest (estimated from the historical mapping of the Santarém City Hall). This city

quickly expanded, occupying 5.2 $km^2$ by the end of the 1970s and 49.3 $km^2$ currently (estimated from satellite images LANDSAT/SRTM). Jupindá Lake is 70 km East of from Santarém City, and receives surface water inflow from small streams draining from the forest and the main tributary Curuá-Una River, a large affluent of the Amazon River (Figure 1). The Lake has been affected by the deforestation associated with the expansion of Santarém City. Between the 1940's and 1950's, there was intense deforestation on the margins of rivers and streams in this area, used to supply the markets with wood and forestry products (Amorim 2000, Cruz et al. 2011). In the 1970s, the Curuá-Una River was dammed (Curuá-Una Dam) 45 km upstream of Jupindá Lake to build the first hydroelectric plant of the Amazon Forest (LigockI 2003).

A 60 cm depth sediment core (diameter 7.5 cm) was collected in 2010 using a gravity corer in the center of the Jupindá Lake (02°27'43.60" S, 54° 5'1.30" W). The sediment core was sub sampled at 2 cm intervals. Dry bulk density (DBD, g $cm^{-3}$) was determined as the dry sediment weight (g) divided by the initial volume ($cm^3$). A homogenized portion was acidified (10% HCl following the procedures outlined in Naidu et al. (2000)) to remove carbonate material, then dried and ground to powder for organic carbon (OC), nitrogen (N), $\delta^{13}C$, and $\delta^{15}N$ analyses using a Flash Elemental Analyzer coupled to a Thermo Fisher Delta V IRMS (isotope ratio mass spectrometer). Working standards were used (glucose, 10.7 ppt and urea, 41.3 ppt) to calibrate for $\delta^{13}C$. A pair of standards were measured with every 20 samples. These standards were calibrated initially against international absolute standards LSVEC and NIST8542. Analytical precision: C = 0.1 %, N = 0.1%, $\delta^{13}C$ = 0.1‰ and $\delta^{15}N$ = 0.15 ‰.

Samples were prepared for Pu dating following the method of Ketterer et al. (2004) with modifications to enable larger sample mass to be processed as a result of the likely lower Pu concentrations in the Southern Hemisphere (Sanders et al. 2016). To obtain a larger mass, sediment intervals were joined and homogenized so the sediment intervals for the $^{240+239}$Pu dating was 4 cm intervals. Sample aliquots ranging from 14 to 29 grams were dry-ashed at 600 $^{O}$C for 16 hours, and leached with 50 mL of 16 M $HNO_3$. The leaching was conducted overnight at 80$^{O}$C with added $^{242}$Pu yield tracer (NIST 4334g, 19 picograms). Acid leaching (as opposed to complete dissolution with HF) is known to solubilize stratospheric fallout Pu, and there is little possibility that "refractory" $HNO_3$-insoluble Pu exists in the South America (Sanders et al. 2014). The leachates were diluted to 100 mL, filtered to remove solids, and the aqueous solutions were processed with TEVA resin (EIChrom, Lisle, Il, USA) in order to chemically isolate 3.0 mL Pu fractions in aqueous ammonium oxalate solution suitable for measurements by sector ICPMS. Pu determinations were performed using a VG Axiom MC operating in the single collector (electron multiplier) mode. The system was used with an APEX HF desolvating micronebulizer system (ESI Scientific, Omaha, NE, USA) with an uptake rate of 0.4 mL/minute. Qualitative mass spectral scans (averages of 50 sweeps over the mass range 237.4 – 242.6) were collected for selected samples prior to the electrostatic sector quantitative scanning of $^{238}$U+, $^{239}$Pu+, $^{240}$Pu+, and $^{242}$Pu+. Detection limits were evaluated based upon the analysis of two blanks and considerations regarding the obtained mass spectra. A detection limit of 0.01 Bq/kg of $^{239+240}$Pu is applicable for samples of nominal 25 g mass.

For $^{210}$Pb dating, an intrinsic germanium detector coupled to a multi-channel analyzer was used. Freeze dried and ground sediments were packed and sealed in gamma tubes. Lead-210 and $^{226}$Ra activities were calculated by multiplying the counts per minute by a factor that includes the gamma-ray intensity and detector efficiency determined from standard calibrations. Identical geometry was used for all samples. Lead-210 activities were determined by the direct measurement of the 46.5 KeV gamma peak. Radium-226 activity was determined via the $^{214}$Pb daughter at 351.9 KeV. For $^{226}$Ra measurements, the packed samples were set aside for at least 21 days to allow for $^{222}$Rn to ingrow and establish secular equilibrium between $^{226}$Ra and its granddaughter $^{214}$Pb. Excess $^{210}$Pb activity was calculated by subtracting the supported $^{210}$Pb (i.e., $^{226}$Ra activity) from the total $^{210}$Pb activity. The sediment accretion rate for the previous 120 years was estimated by two methods derived from $^{210}$Pb dating, the Constant Initial Concentration (CIC) model assuming that this rate has not varied during the encompassed time span (Appleby and Oldfield 1992), and the Constant Rate of Supply (CRS) model based on a constant influx of unsupported, atmospheric $^{210}$Pb that allows a variable sediment rate (Ivanovich and Harmon 1992). Organic carbon accumulation rates were estimated from an average between these the two dating methods ($^{239+240}$Pu and $^{210}Pb_{ex}$) the dry bulk density (g cm$^{-3}$) and carbon content for each interval of the entire sediment core.

The land/use cover analysis was based on documented historical information before 1975 and satellite images (Landsat/SRTM, Table 1) from 1975, 1985, 1995 and 2008 available from the United States Geological Survey (USGS). No significant deforestation occurred in the catchment area of the Jupindá Lake until early 1940's (Amorim 2000, Cruz et al. 2011). Subsequent land/use changes were determined using satellite images

169 (Gordon 1980, Munyati 2000). All satellite images were from low-water seasons to
170 remove the influence of the flood pulse on the exposed area over years. The resolution of
171 the images was 30 m, except that from the 1970's which was resampled from 90 to 30 m
172 (Table 1). This approach allowed an assessment of changes in land cover which could
173 then be compared to results from carbon accumulation. Results of the spatial assessment
174 were separated into two time periods; 1934-1975, or the timeframe between the onset of
175 land clearing and the first satellite image, and 1975-2008 which provides a more detailed
176 assessment of temporal changes to the study area. The time period 1934-1975 was
177 characterized by a rapid removal (peak until the 1960's) of vegetation established at the
178 margins of inland waters; especially *Aniba rosaeodora* (Pau-rosa) for extraction of oils,
179 and *Mezilaurus itauba* and *Cedrela fissilis* (Louro-itaúba and Cedro, respectively) as
180 hardwoods, and the opening of clearings for crops of textile fibers and subsistence
181 products. Further, intensification of deforestation towards the interior of the forest and
182 following the urban growth of Santarém is reported from the 1970's (Amorim 2000, Cruz
183 et al. 2011). The depleting vegetal resources near to the margins of lakes and running
184 waters in this region is also well documented (Amorim 2000, Cruz et al. 2011).

185 In order to address the spatial dependence of recent OC burial in Jupindá Lake for
186 deforestation, we analyzed the land/cover use in four buffer areas around this lake and
187 contributing rivers or streams. The first buffer of 100 m represented the riparian forest
188 protected area by the Brazilian laws for fluvial channels with a width of 50 to 200 m.
189 Other buffers were progressively higher, with a width of 500, 1000 and 6000 m from the
190 riverbank and lake margins (Figure 2). In addition, we considered only stretches of rivers
191 and streams 65-km long from Jupindá Lake to analyze its catchment area of more direct

192 influence. This criteria also avoids the interference of the artificial flooding on the
193 margins of the Curuá-Una hydroelectric dam, which was built in 1977 (Fearnside 2005).
194 All the statistical tests used in this work were performed using GraphPad Prism 5.0
195 software.
196
197 **3. Results**
198 The analyses of $^{239+240}$Pu showed no detectable activities from the bottom of the
199 sediment core until the 22-26 cm interval (Figure 3). However, $^{239+240}$Pu was detected in
200 the 18-22 cm interval (0.029 ± 0.002 Bq/kg $^{239+240}$Pu) with the highest concentrations
201 (0.047 ± 0.004 Bq/kg $^{239+240}$Pu) at the 16 cm depth. The $^{239+240}$Pu activities appears to
202 spike at the 14 to 18 cm interval, which indicates the 1963 stratospheric fallout peak. It
203 may be said with certainty that the material below 22 cm was deposited pre-bomb (that is,
204 prior to the early 1950's). This affixes an upper limit on the average sedimentation rate of
205 near to 3.8 mm year$^{-1}$. The Pu atom ratio data indicate that the Pu is originating from
206 stratospheric fallout, i.e. plutonium isotopic ratios ($^{240/239}$Pu) of ~0.18. These results are
207 consistent with the $^{240}$Pu$^{/239}$Pu of 0.180 ± 0.014 discussed by Kelley et al. (1999).
208 The $^{210}$Pb and $^{226}$Ra profiles as well as the $^{210}$Pb$_{(ex)}$ profile vs cumulative dry mass
209 accumulation reveals a complex depositional environment with sedimentation variations
210 in the upper intervals with disturbances, such as bio-turbation and resuspension in the
211 upper ~ 20 cm of the sediment column (Figure 4). A decrease in $^{210}$Pb$_{ex}$ activity was
212 found below the 20 cm depth interval. The $^{210}$Pb$_{ex}$ data distribution are as follows: y = -
213 0.0749x + 7.5; $R^2$ = 0.73; n=19; p < 0.01 from the 20 to the 60 cm interval, below the
214 apparent mixed zone. This indicates that the sedimentation is constant below the 20 cm

depth. Both estimates of sediment accretion rate during the 120 years from CIC and CRS models were similar, reaching 4.1 and 4.3 mm $yr^{-1}$ respectively, which were slightly higher than the ~ 60 year $^{239+240}Pu$ dates (3.8 mm $yr^{-1}$). In order to obtain a more reliable estimates of the historical carbon burial rates, an average was taken between these the two dating methods, $^{239+240}Pu$ and $^{210}Pb_{ex}$ (4 mm $year^{-1}$), and multiplied by the DBD and OC content for each interval of the entire sediment core.

Because the $^{210}Pb_{ex}$ activities are relatively uniform from the surface to the ~20 cm depth, the short-term measurements are not possible. However, from the $^{239+240}Pu$ data, one can say with certainty that the material below 22 cm was deposited pre-bomb (that is, prior to the early 1950s). This affixes an upper limit on the sedimentation accumulation rate (SAR), form 1950 to 2010, to be near 3.8 cm/year. This accretion rate is similar to the $^{210}Pb$ rates and we therefore conclude that the sedimentation rates have not changed significantly during previous ~120 years.

The dry bulk density (DBD), total organic carbon (OC%), total nitrogen (TN%) content as well as the carbon and nitrogen (C/N) molar ratios along with the $\delta^{13}C$ and $\delta^{15}N$ values showed a shift towards the center of the sediment core (Table 2). The relationship between $\delta^{13}C$ and $\delta^{15}N$ indicated different origins of OC in the sediment core (Figure 5) contributing to the significant relationship between OC burial and the $\delta^{13}C$ (Figure 6). The significantly greater $\delta^{13}C$ peak and lower $\delta^{15}N$ values coupled to higher OC burial rates were observed in the phase between 1934-1975 in Jupindá Lake (one-way ANOVA followed by Tukey's post test, $p<0.05$; Fig. 7). The $\delta^{13}C$ values were greater in the phase 1934-1975 in relation to those previous and after respectively (one-way ANOVA followed by Tukey's post test, $p<0.05$). This peak between 1934-1975 also

238 showed $\delta^{15}N$ values lower and OC burial rates higher than other phases (one-way
239 ANOVA followed by Tukey's post test, $p<0.05$).

240 The OC burial rates indicate an increasing trend from ~ 1930 to 1960 with a peak
241 during the 1940's and 50's (grey area in Figure 7). The carbon burial rates increased,
242 from ~142 g $m^{-2}$ $year^{-1}$ in the time period 1890 – 1940, and up to 298 g $m^{-2}$ $year^{-1}$
243 between 1940 and 1950. Carbon accumulation then decreased to approximately 218 g $m^{-2}$
244 $year^{-1}$ from 1960 to 1980, after which a gradual decline in carbon burial is noted. In
245 relation to land use/cover in the surrounding fluvial channels and the Jupindá lake, only
246 the smallest buffer (100 m) showed significant changes during 1934-1975. This time
247 period is when deforestation was nearly 75% higher than in the subsequent time period
248 1975-2008 (Figure 8a) and when OC burial was greatest ((Figure 8b).
249

250 **4. Discussion**

251 Overall, similar estimates of sediment accretion were found using different
252 methodologies ($^{239+240}Pu$ and $^{210}Pb_{(ex)}$). These accretion rates along with the dry bulk
253 density revealed an insight into changes in the sediment sources. This indicates that even
254 though the origin of the sediment may have been modified, the sediment accumulation
255 has varied little as indicated by the ~60 and 120 year rates.

256 The high peak in carbon accumulation observed around 1950 appears to be associated
257 with a shift in the source of organic material, inferred by changes in carbon and nitrogen
258 contents and the isotopic fractioning toward the middle (from 20 to 40 cm depth interval)
259 of the sediment column. This peak for different organic and inorganic variables in
260 intermediate depths revealed changes not only in the amount but also in the type of

material being deposited over time. Previous studies have reported two common origins for OC in the Amazon forest. Higher $\delta^{15}N$ and more negative $\delta^{13}C$ values could indicate the presence of Santarém soil organic matter (such as that adjacent to the Jupindá Lake), while lower $\delta^{15}N$ and more variable $\delta^{13}C$ values indicate particulate organic carbon (POC) from the terrestrial vegetation in the catchment (Ometto et al. 2006, Zocatelli et al. 2013). Here, a corresponding increase in OC%, TN% and OC burial rates measured, with a peak near 1950, suggesting higher inputs of organic matter into lake. The higher $\delta^{13}C$ signature, coupled with a lower $\delta^{15}N$ indicates a greater influence from the terrestrial Amazonian POC during the same period, around 1950 (Ometto et al., 2006).

The statistical treatment of variables and OC burial rates, when grouped into different phases, showed assumptions which required parametric analyses, including normal distribution (Kolmogorov-Smirnov, $p > 0.05$) and homogeneity of variance (Bartlett, $p > 0.05$). Thus, we used means and standard errors to represent the distribution of values, and parametric tests were conducted to compare different phases. Statistical differences were tested using the one-way ANOVA test followed by Tukey's post test (significance was defined as $p < 0.05$). The stable isotope results and OC burial rates, when grouped into different phases, showed assumptions required for parametric analyses, including normal distribution (Kolmogorov-Smirnov, $p > 0.05$) and homogeneity of variance (Bartlett, $p > 0.05$) (Figure 7). Thus, when examining the means and standard errors to represent the distribution of values, and parametric tests, different sedimentary phases are noted. These different sedimentary phases are confirmed by statistical differences as tested using a one-way ANOVA test followed by Tukey's post test (significance was defined as $p < 0.05$).

When looking for a cause for this change in the source of organic material, we look to the analysis of land use change. Land clearing associated with early occupation from the 1940s in the catchment area of the Jupindá Lake reveals a potential cause of the increased carbon burial observed in this lake. Changes in development use and forestation may significantly affect recent OC burial in mid-high-latitude lakes (Anderson et al. 2013, Dietz et al. 2015). Indeed, our results suggest that land clearing during the 1940's and 50's might be related to increased organic matter deposition in the region's floodplain lakes. During this period, intense wood extraction and expansion of agricultural settlements occurred (Amorim 2000, Cruz et al. 2011). One important consequence of deforestation in the watershed is the silting up of lakes (Enea et al. 2012 ), including those at humid low-latitude areas (Cohen et al. 2005, Bakoariniaina et al. 2006). However, the lake is in a region relatively preserved, and therefore there is no other explanation other than deforestation in the margins to have caused the peak in OC burial between 1934 and 1975. The riparian forest systems are generally effective in reducing the sediment transport by surface runoff, with the removal of this vegetation increasing the erosion processes especially in the Amazon Basin as a result of intense rainfall (Neill et al. 2013a). The peak of the significantly greater $\delta^{13}C$ and lower $\delta^{15}N$ values coupled to higher OC burial rates were observed in the phase between 1934-1975 in Jupindá Lake (one-way ANOVA followed by Tukey's post test, $p<0.05$; Fig. 7). The $\delta^{13}C$ values were greater in the 1934-1975 phase as related to those previous and after respectively (one-way ANOVA followed by Tukey's post test, $p<0.05$). This peak between 1934-1975 also showed delta $\delta^{15}N$ values lower and OC burial rates higher than other phases (one-way ANOVA followed by Tukey's post test, $p<0.05$).

We also found a spatial dependence of the carbon accumulation in the Lake Jupindá, as the much lower OC burial was coupled to higher deforestation rates in those larger buffers around its margins and main fluvial channels (500, 1000 and 6000 m) in the period after 1975 (1975-2008) than that before (1934-1975). This confirms previous evidences that the recent deforestation process in the region was started in areas near running and lake waters (Amorim 2000, Cruz et al. 2011), and not in the interior of the forest. The enhanced OC burial in lacustrine sediments before 1975 was related to higher deforestation rates only in the riparian vegetation zone (100-m buffers), suggesting a higher influence of deforestation with decreasing distance to water courses. Therefore, the soil carbon enrichment to the aquatic sediments during the peaks of riparian deforestation may cause intense but temporary carbon burial events in the Amazon floodplain, representing a significant part of the total loss of terrestrial organic matter. In contrast, the continued removal of vegetation from the interior of the forest might be not directly related to increases of OC burial, even temporarily, in depositional aquatic ecosystems.

## 5. Conclusion

The $^{239+240}$Pu and $^{210}$Pb dating methods were combined with a spatial analysis of vegetation clearing to firstly calculate carbon accumulation rates, and then to interpret changes in sediment characteristics during the previous century. The Pu dating method closely approximates measurements from the $^{210}$Pb chronologies and hence offers mechanism to determine sedimentation rates and carbon accumulation in Amazon sediments. An increase in OC burial, up to 319 OC g $m^{-2}$ $year^{-1}$, coincides with changes

330 in the $\delta^{13}C$ and $\delta^{15}N$ signatures, likely influenced by the heavy deforestation in riparian
331 systems of this region during the 1940s and 50's. It is therefore suggested that the net
332 increase in carbon burial towards the center of the sediment core, which represents the
333 highest carbon burial rates during the 1950s, is a result of a change in source of organic
334 matter deposition. The differing carbon burial rates along the sediment core reveals the
335 potential complexity of the Amazon floodplain lakes, directly related to the development
336 within the Basin. This work demonstrates a new understanding on spatial dependence of
337 carbon burial capacity of the Amazon floodplain lakes with respect to advances in
338 deforestation in the Basin.
339
340 **Acknowledgements**
341 LMS is supported by an APA and IPRS scholarships. HM received a research grant from
342 the Brazilian Research Council (CNPq – "Programa Universal") and the Research
343 Support Foundation of the State of Rio de Janeiro (FAPERJ – "Programa Jovem Cientista
344 do Nosso Estado"). CJS is supported by the Australian Research Council (DE160100443
345 and LE140100083).
346
347 **CAPTIONS TO FIGURES**
348 **Figure 1.** Floodplain Lake where the sediment core was collect, near the Amazon River
349 and the city of Santarém, Brazil. This floodplain lake has a diameter of approximately 3
350 km.
351 **Figure 2.** Different buffer sizes (100m, 500m, 1km and 6km) along the stretch of the
352 Curuá-Una river from Jupindá Lake (red) to the hydroelectric dam upstream (yellow).

**Figure 3.** $^{239+240}$Pu profile, indicating ~ 1950 when these radionuclides were first introduced into the atmosphere.

**Figure 4.** Lead-210 (black circles) and $^{226}$Ra (white circles) profiles against depth. Grey squares represent the $^{210}$Pb(ex) profile vs cumulative dry mass.

**Figure 5.** $\delta^{13}C$ vs $\delta^{15}N$. The Amazon River POM and Santarem soil organic matter values, adjacent to the study area, are taken from Zocatelli et al (2013).

**Figure 6.** Carbon burial as a function of $\delta^{13}C$ and $\delta^{15}N$.

**Figure 7**. $\delta^{13}C$, $\delta^{15}N$ and carbon burial rate values in relation to age (year). Panels below each vertical profile represent respective data grouped by the phases >1934, 1934-1975 and 1975-2008. Filled square symbols represent means of a given variable in each sediment layer, and the vertical bars show the mean with the standard deviation of the respective phase. Equal letters in each panel represent non-significant differences ($p >$ 0.05, one-way ANOVA followed by Tukey's post test).

**Figure 8.** Percentage of modified areas in relation to the different buffers (Panel A). Carbon burial (black dots) and changes in the riparian vegetation (grey bars) as related to time (Panel B).

**CAPTION TO TABLES**

**Table 1**. Satellite acquisition data from United States Geological Survey (USGS) and the Curuá-Una River quota from Brazilian Water Agency (ANA).

**Table 2.** Depth profiles of dry bulk density (DBD), total organic carbon (OC%), total nitrogen (TN%) carbon and nitrogen (C/N) molar ratios, $\delta^{13}C$ and $\delta^{15}N$.

**Table 1.**

| *Month/Year* | *Landsat Data* | *Curuá-Una River Quote* |
|---|---|---|
| Aug/1975 | 2 | 5.3 |
| Oct/1985 | 5 | 3.7 |
| June/1995 | 5 | 6 |
| June/2008 | 5 | *No data* |

**Table 2.**

| Depth (cm) | DBD (g $cm^{-3}$) | $\delta^{15}N$ | $\delta^{13}C$ | C (%) | N (%) | C/N |
|---|---|---|---|---|---|---|
| 0-2 | 1.0 | 8.9 | -29.2 | 3.8 | 0.3 | 17.2 |
| 2-4 | 0.9 | 11.7 | -29.0 | 3.8 | 0.3 | 18.7 |
| 4-6 | 1.0 | 10.4 | -28.8 | 4.0 | 0.3 | 19.2 |
| 6-8 | 1.1 | 9.3 | -28.7 | 4.3 | 0.3 | 20.2 |
| 8-10 | 1.0 | 9.4 | -28.7 | 4.1 | 0.3 | 19.8 |
| 10-12 | 1.1 | 7.9 | -28.6 | 4.6 | 0.3 | 21.2 |
| 12-14 | 1.1 | 8.2 | -28.7 | 4.3 | 0.3 | 19.9 |
| 14-16 | 1.1 | 7.8 | -28.6 | 4.3 | 0.3 | 20.9 |
| 16-18 | 1.0 | 8.7 | -28.5 | 4.4 | 0.3 | 21.2 |
| 18-20 | 1.1 | 7.5 | -28.4 | 4.4 | 0.3 | 19.8 |
| 20-22 | 1.0 | 6.5 | -28.2 | 5.4 | 0.3 | 21.2 |
| 22-24 | 1.0 | 6.0 | -27.8 | 5.3 | 0.3 | 21.5 |
| 24-26 | 1.0 | 5.2 | -27.4 | 7.3 | 0.4 | 25.4 |
| 26-28 | 1.1 | 6.1 | -27.6 | 6.0 | 0.3 | 23.8 |
| 28-30 | 1.0 | 5.0 | -27.3 | 6.0 | 0.4 | 22.7 |
| 30-32 | 1.0 | 5.4 | -28.0 | 6.1 | 0.3 | 27.0 |
| 32-34 | 1.3 | 6.6 | -28.5 | 4.4 | 0.2 | 27.5 |
| 34-36 | 1.6 | 8.9 | -29.0 | 2.2 | 0.1 | 23.1 |
| 36-38 | 1.4 | 11.4 | -29.4 | 2.9 | 0.1 | 30.4 |
| 38-40 | 1.4 | 10.4 | -29.5 | 3.3 | 0.1 | 30.5 |
| 40-42 | 1.5 | 11.4 | -29.3 | 2.4 | 0.1 | 23.8 |
| 42-44 | 1.6 | 12.2 | -29.4 | 1.3 | 0.1 | 15.6 |
| 44-46 | 1.8 | 8.2 | -29.6 | 1.2 | 0.1 | 14.3 |
| 46-48 | 1.5 | 8.8 | -29.8 | 2.2 | 0.1 | 21.6 |
| 48-50 | 0.9 | 10.4 | -29.7 | 2.9 | 0.2 | 25.6 |
| 50-52 | 0.9 | 10.2 | -29.7 | 2.6 | 0.1 | 27.2 |
| 52-54 | 0.9 | 7.1 | -29.7 | 3.9 | 0.2 | 28.6 |
| 54-56 | 0.9 | 9.2 | -29.9 | 3.6 | 0.2 | 27.8 |
| 56-58 | 0.9 | 6.6 | -30.1 | 4.3 | 0.2 | 30.1 |
| 58-60 | 0.9 | 5.0 | -30.1 | 3.5 | 0.2 | 23.1 |
| **Average** | **1.11** | **8.34** | **-28.9** | **4.0** | **0.2** | **23.0** |
| **Stand Dev** | **0.24** | **2.1** | **0.8** | **1.9** | **0.1** | **4.2** |

435 **References**
436
437 Aalto, R., L. Maurice-Bourgoin, T. Dunne, D. R. Montgomery, C. A. Nittrouer, and J. L.
438 Guyot. 2003. Episodic sediment accumulation on Amazonian flood plains
439 influenced by El Niño/Southern Oscillation. Nature **425**:493-497.
440 Abril, G., J. M. Martinez, L. F. Artigas, P. Moreira-Turcq, M. F. Benedetti, L. Vidal, T.
441 Meziane, J. H. Kim, M. C. Bernardes, N. Savoye, J. Deborde, E. L. Souza, P.
442 Albéric, M. F. Landim De Souza, and F. Roland. 2014. Amazon River carbon
443 dioxide outgassing fuelled by wetlands. Nature **505**:395-398.
444 Amorim, A. T. d. S. 2000. Santarém: uma síntese histórica, Canoas, Ulbra, Santarem,
445 Brazil
446 Anderson, N. J., R. D. Dietz, and D. R. Engstrom. 2013. Land-use change, not climate,
447 controls organic carbon burial in lakes. Proceedings. Biological sciences / The
448 Royal Society **280**:20131278.
449 Appleby, P. G., and F. Oldfield. 1992. Application of lead-210 to sedimentation studies.
450 Pages 731-783 *in* M. Ivanovich and S. Harmon, editors. Uranium Series
451 Disequilibrium: Application to Earth, Marine and Environmental Science. Oxford
452 Science Publications.
453 Bakoariniaina, L. N., T. Kusky, and T. Raharimahefa. 2006. Disappearing Lake Alaotra:
454 Monitoring catastrophic erosion, waterway silting, and land degradation hazards
455 in Madagascar using Landsat imagery. Journal of African Earth Sciences **44**:241-
456 252.
457 Cohen, A. S., M. R. Palacios-Fest, J. McGill, P. W. Swarzenski, D. Verschuren, R.
458 Sinyinza, T. Songori, B. Kakagozo, M. Syampila, C. M. O'Reilly, and S. R. Alin.
459 2005. Paleolimnological investigations of anthropogenic environmental change in

Lake Tanganyika: I. An introduction to the project. Journal of Paleolimnology **34**:1-18.

Cruz, H., P. Sablayrolles, M. Kanashiro, and M. S. Amaral, P. 2011. Relação empresa/ comunidade no manejo florestal comunitário e familiar: Uma contribuição do Projeto Floresta em pé.

Diaz, R. J., and R. Rosenberg. 2008. Spreading dead zones and consequences for marine ecosystems. Science **321**:926-929.

Dietz, R. D., D. R. Engstrom, and N. J. Anderson. 2015. Patterns and drivers of change in organic carbon burial across a diverse landscape: Insights from 116 Minnesota lakes. Global Biogeochemical Cycles **29**:708-727.

Dong, X., N. J. Anderson, X. Yang, X. chen, and J. Shen. 2012. Carbon burial by shallow lakes on the Yangtze floodplain and its relevance to regional carbon sequestration. Global Change Biology **18**:2205-2217.

Downing, J. P., M. Meybeck, J. C. Orr, R. R. Twilley, and H. W. Scharpenseel. 1993. Land and water interface zones. Water, Air, & Soil Pollution **70**:123-137.

Enea, A., G. Romanescu, and C. Stoleriu. 2012 Quantitative considerations concerning the source-areas for the silting of the red lake (Romania) lacustrine basin.

. Romania.

Fearnside, P. M. 2005. Do hydroelectric dams mitigate global warming? The case of Brazil's Curuá-Una Dam. Mitigation and Adaptation Strategies for Global Change **10**:675-691.

Gordon, S. I. 1980. Utilizing LANDSAT imagery to monitor land-use change: A case study in ohio. Remote Sensing of Environment **9**:189-196.

483 Goulding, M. 1993. Flooded forests of the Amazon. Scientific American **268**:114-
484 120+115.
485 Hoffmann, T., M. Schlummer, B. Notebaert, G. Verstraeten, and O. Korup. 2013. Carbon
486 burial in soil sediments from Holocene agricultural erosion, Central Europe.
487 Global Biogeochemical Cycles **27**:828-835.
488 INPE. 2016. Program for the Estimation of Amazon Deforestation. Accessed 20
489 November 2016, http://www.obt.inpe.br/prodes/prodes_1988_2015n.htm.
490 Ivanovich, M., and S. Harmon. 1992. Uranium Series Disequilibrium - Applications to
491 Earth, Marine and Environmental Sciences. second edition edition. Oxford
492 Science Publications.
493 Junk, W. J. 2013. Current state of knowledge regarding South America wetlands and
494 their future under global climate change. Aquatic Sciences **75**:113-131.
495 Ketterer, M. E., K. M. Hafer, V. J. Jones, and P. G. Appleby. 2004. Rapid dating of
496 recent sediments in Loch Ness: Inductively coupled plasma mass spectrometric
497 measurements of global fallout plutonium. Science of the Total Environment
498 **322**:221-229.
499 LigockI, L. P. 2003. Comportamento geotécnico da barragem de Curuá-Una, Pará. Rio de
500 Janeiro.
501 Lucas, C. M., J. Schöngart, P. Sheikh, F. Wittmann, M. T. F. Piedade, and D. G.
502 McGrath. 2014. Effects of land-use and hydroperiod on aboveground biomass and
503 productivity of secondary Amazonian floodplain forests. Forest Ecology and
504 Management **319**:116-127.

505 Marotta, H., L. Bento, F. A. De Esteves, and A. Enrich-Prast. 2009. Whole ecosystem
506 evidence of eutrophication enhancement by wetland dredging in a shallow
507 Tropical Lake. Estuaries and Coasts **32**:654-660.
508 Marotta, H., C. M. Duarte, F. Meirelles-Pereira, L. Bento, F. A. Esteves, and A. Enrich-
509 Prast. 2010. Long-term CO2 variability in two shallow tropical lakes experiencing
510 episodic eutrophication and acidification events. Ecosystems **13**:382-392.
511 Marotta, H., L. Pinho, C. Gudasz, D. Bastviken, L. J. Tranvik, and A. Enrich-Prast. 2014.
512 Greenhouse gas production in low-latitude lake sediments responds strongly to
513 warming. Nature Climate Change **4**:467-470.
514 Melack, J. M., L. L. Hess, M. Gastil, B. R. Forsberg, S. K. Hamilton, I. B. T. Lima, and
515 E. M. L. M. Novo. 2004. Regionalization of methane emissions in the Amazon
516 Basin with microwave remote sensing. Global Change Biology **10**:530-544.
517 Munyati, C. 2000. Wetland change detection on the Kafue Flats, Zambia, by
518 classification of a multitemporal remote sensing image dataset. International
519 Journal of Remote Sensing **21**:1787-1806.
520 Naidu, A. S., L. W. Cooper, B. P. Finney, R. W. Macdonald, C. Alexander, and I. P.
521 Semiletov. 2000. Organic carbon isotope ratio (δ13C) of Arctic Amerasian
522 Continental shelf sediments. International Journal of Earth Sciences **89**:522-532.
523 Neill, C., M. T. Coe, S. H. Riskin, A. V. Krusche, H. Elsenbeer, M. N. Macedo, R.
524 McHorney, P. Lefebvre, E. A. Davidson, R. Scheffler, A. M. e Silva Figueira, S.
525 Porder, and L. A. Deegan. 2013a. Watershed responses to Amazon soya bean
526 cropland expansion and intensification. Philosophical Transactions of the Royal
527 Society B: Biological Sciences **368**.

528 Neill, C., M. T. Coe, S. H. Riskin, A. V. Krusche, H. Elsenbeer, M. N. Macedo, R.
529 McHorney, P. Lefebvre, E. A. Davidson, R. Scheffler, A. M. Figueira, S. Porder,
530 and L. A. Deegan. 2013b. Watershed responses to Amazon soya bean cropland
531 expansion and intensification. Philosophical transactions of the Royal Society of
532 London. Series B, Biological sciences **368**:20120425.
533 Neue, H. U., J. L. Gaunt, Z. P. Wang, P. Becker-Heidmann, and C. Quijano. 1997.
534 Carbon in tropical wetlands. Geoderma **79**:163-185.
535 Ometto, J. P. H. B., J. R. Ehleringer, T. F. Domingues, J. A. Berry, F. Y. Ishida, E.
536 Mazzi, N. Higuchi, L. B. Flanagan, G. B. Nardoto, and L. A. Martinelli. 2006.
537 The stable carbon and nitrogen isotopic composition of vegetation in tropical
538 forests of the Amazon Basin, Brazil. Biogeochemistry **79**:251-274.
539 Peixoto, R. B., H. Marotta, D. Bastviken, and A. Enrich-Prast. 2016. Floating Aquatic
540 Macrophytes Can Substantially Offset Open Water CO<inf>2</inf> Emissions
541 from Tropical Floodplain Lake Ecosystems. Ecosystems **19**:724-736.
542 Sanders, C. J., B. D. Eyre, I. R. Santos, W. MacHado, W. Luiz-Silva, J. M. Smoak, J. L.
543 Breithaupt, M. E. Ketterer, L. Sanders, H. Marotta, and E. Silva-Filho. 2014.
544 Elevated rates of organic carbon, nitrogen, and phosphorus accumulation in a
545 highly impacted mangrove wetland. Geophysical Research Letters **41**:2475-2480.
546 Sanders, C. J., I. R. Santos, D. T. Maher, J. L. Breithaupt, J. M. Smoak, M. Ketterer, M.
547 Call, L. Sanders, and B. D. Eyre. 2016. Examining 239+240Pu, 210Pb and
548 historical events to determine carbon, nitrogen and phosphorus burial in
549 mangrove sediments of Moreton Bay, Australia. Journal of Environmental
550 Radioactivity **151**:623-629.

Skole, D., and C. Tucker. 1993. Tropical deforestation and habitat fragmentation in the amazon: Satellite data from 1978 to 1988. Science **260**:1905-1910.

Smith, L. K., J. M. Melack, and D. E. Hammond. 2002. Carbon, nitrogen, and phosphorus content and 210Pb-derived burial rates in sediments of an Amazon floodplain lake. Amazoniana **17**:413-436.

Stanley, E. H., S. M. Powers, N. R. Lottig, I. Buffam, and J. T. Crawford. 2012. Contemporary changes in dissolved organic carbon (DOC) in human-dominated rivers: Is there a role for DOC management? Freshwater Biology **57**:26-42.

Zocatelli, R., P. Moreira-Turcq, M. Bernardes, B. Turcq, R. C. Cordeiro, S. Gogo, J. R. Disnar, and M. Boussafir. 2013. Sedimentary evidence of soil organic matter input to the curuai amazonian floodplain. Organic Geochemistry **63**:40-47.

**Figure 1.**

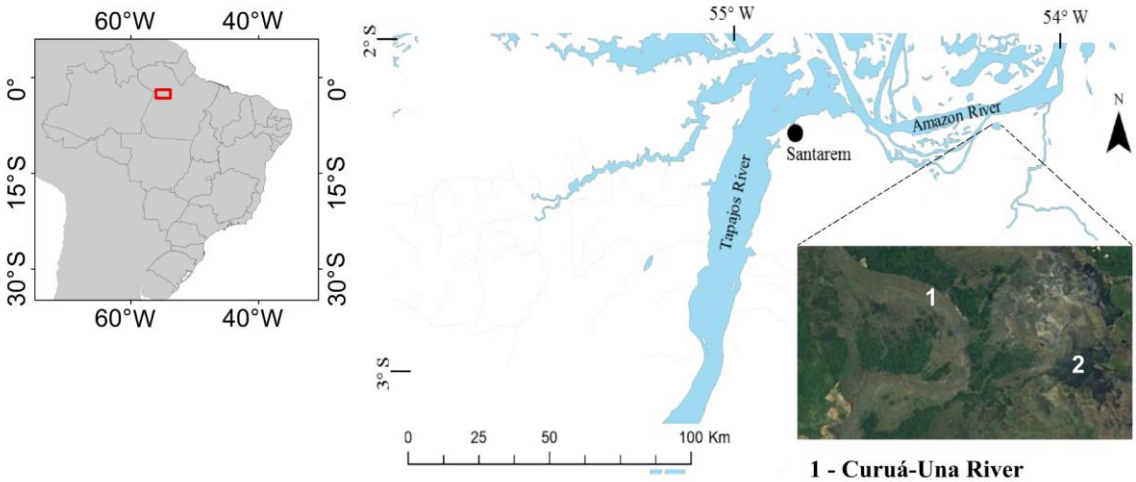
60°W
40°W
0°
15°S
30°S
2° S
3° S
55° W
54° W
N
Amazon River
Santarem
Tapajos River
0
25
50
100 Km
1
2
1 - Curuá-Una River
2 - Floodplain Lake Jupindá

**Figure 2.**

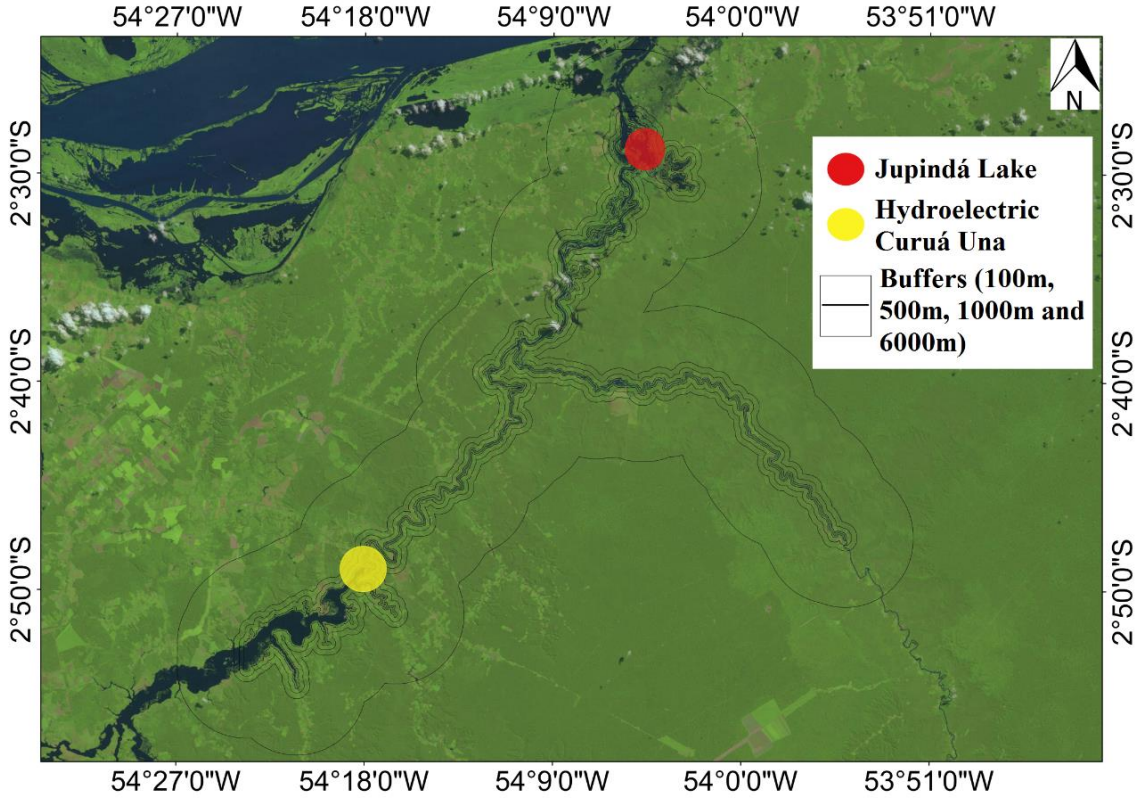
54°27'0"W
54°18'0"W
54°9'0"W
54°0'0"W
53°51'0"W
2°30'0"S
2°40'0"S
2°50'0"S
N
Jupindá Lake
Hydroelectric Curuá Una
Buffers (100m, 500m, 1000m and 6000m)

**Figure 3.**

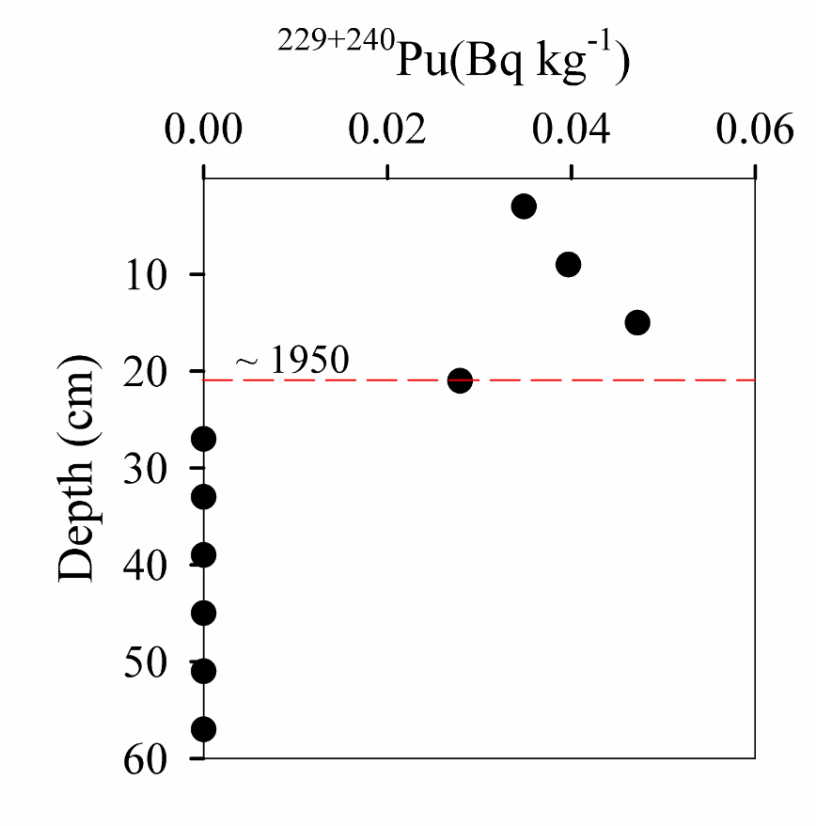

**Figure 4.**

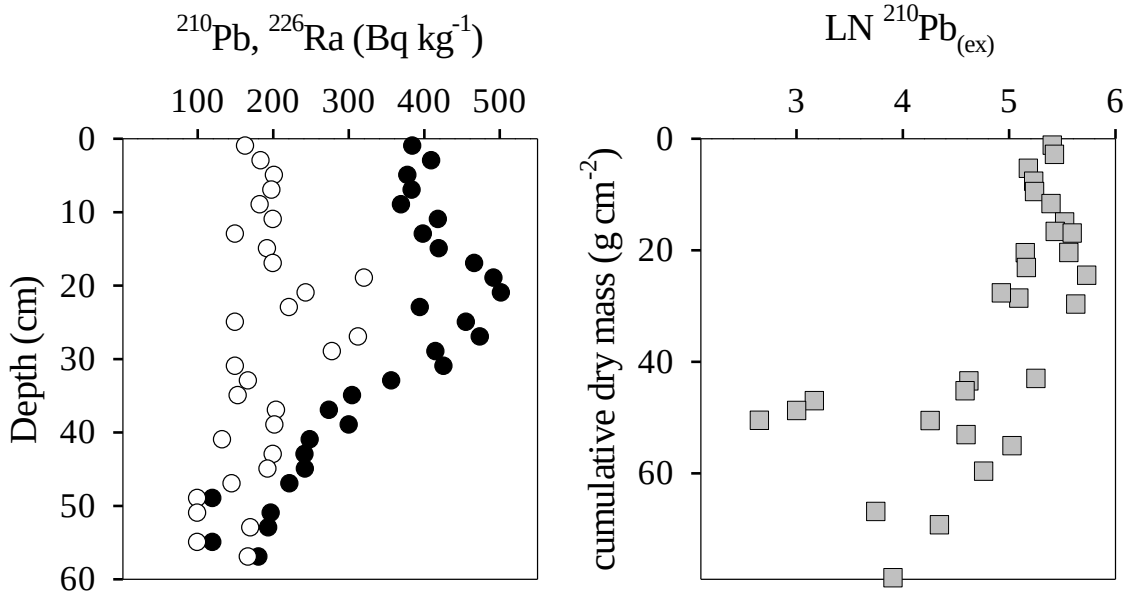
$^{210}$Pb, $^{226}$Ra (Bq kg$^{-1}$)
100 200 300 400 500
Depth (cm)
0 10 20 30 40 50 60
LN $^{210}$Pb$_{(ex)}$
3 4 5 6
cumulative dry mass (g cm$^{-2}$)
0 20 40 60

**Figure 5.**

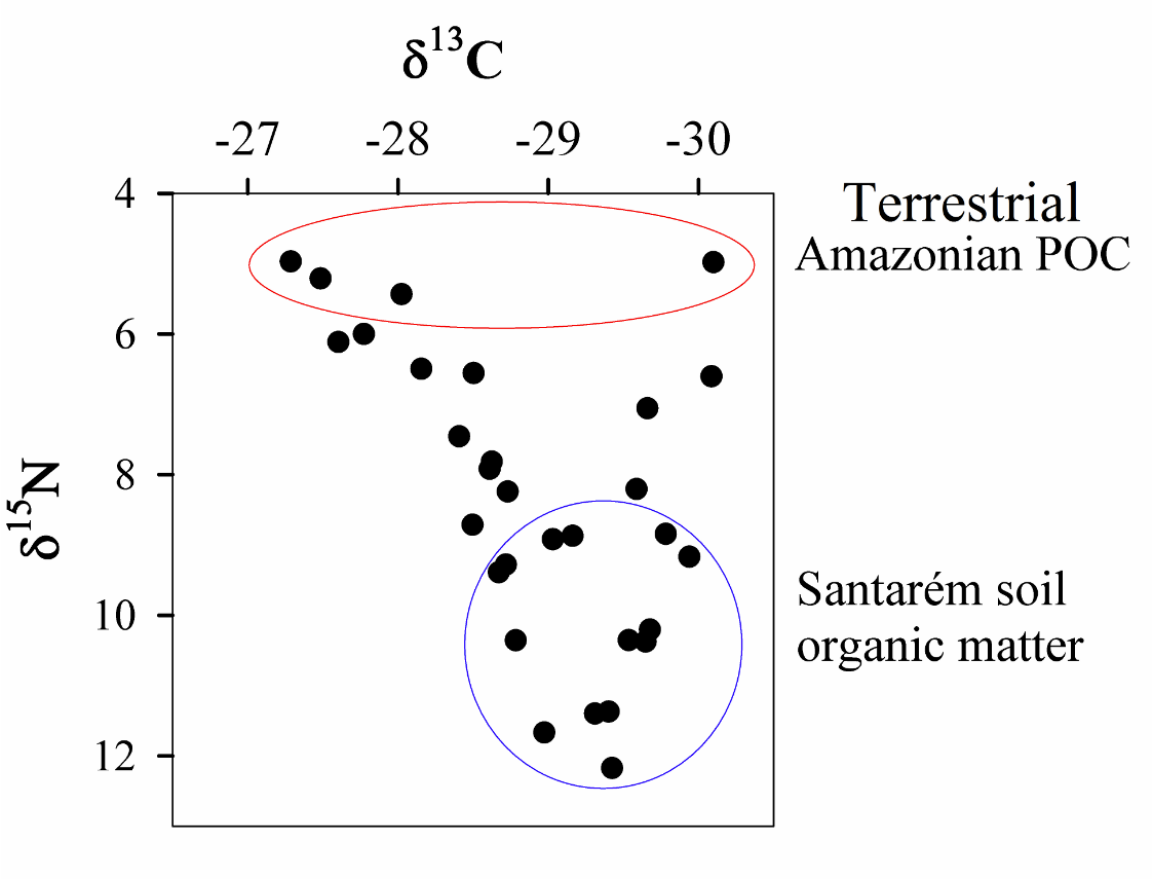
δ13C
-27
-28
-29
-30
4
6
8
10
12
δ15N
Terrestrial
Amazonian POC
Santarém soil
organic matter

**Figure 6.**

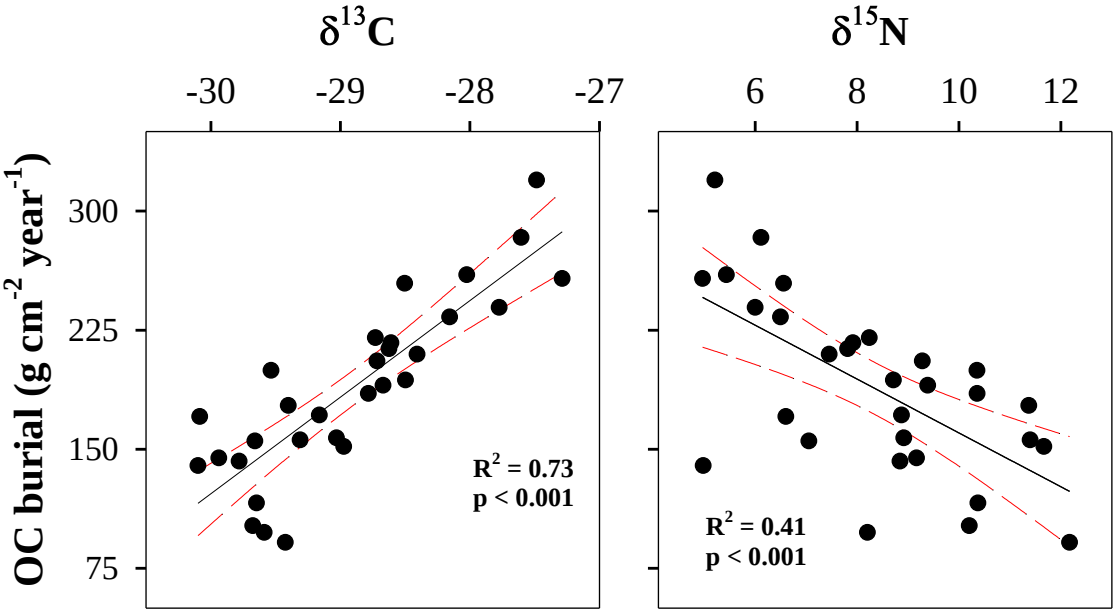
δ13C
δ15N
-30
-29
-28
-27
6
8
10
12
OC burial (g cm-2 year-1)
300
225
150
75
R2 = 0.73
p < 0.001
R2 = 0.41
p < 0.001

**Figure 7.**

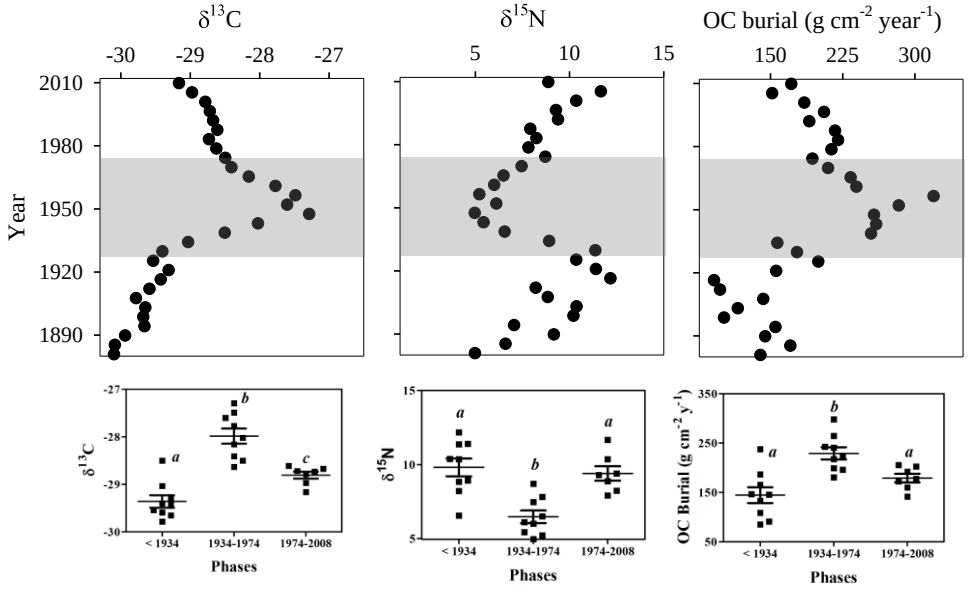
δ13C
δ15N
OC burial (g cm-2 year-1)
-30
-29
-28
-27
5
10
15
150
225
300
2010
1980
1950
1920
1890
Year
δ13C
δ15N
OC Burial (g cm-2 y-1)
a
b
c
< 1934
1934-1974
1974-2008
Phases

772 **Figure 8.**

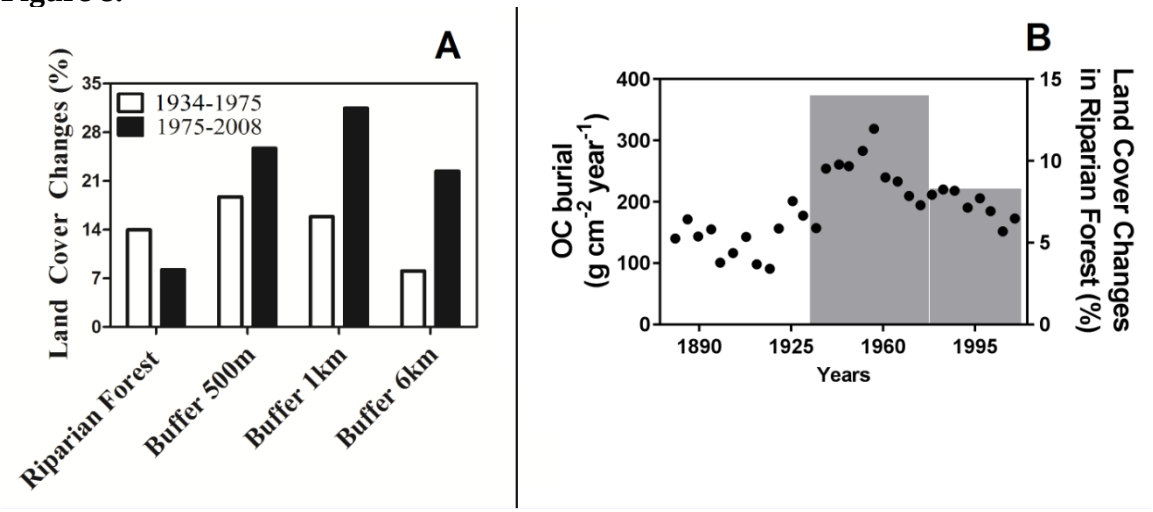


773